Int. J. Solids Structures Vol. 25, No. 1, pp. 23–31, 1989
Printed in Great Britain.

0020-7683/89 $3.00 + .00

SHAPE OPTIMIZATION OF WELD SURFACE

ANDRZEJ SŁUŻALEC
Technical University of Częstochowa, 42-201 Częstochowa, Poland

(*Received* 6 *August* 1987; *in revised form* 11 *June* 1988)

Abstract—In this paper a numerical method for optimizing the shape of a weld surface is presented. The optimal shape design of two cylindrical elements joined by welding is considered in order to minimize the stress concentration factor along the weld. The problem is solved using the finite element method.

INTRODUCTION

In the design process an optimization problem concerning the shape of the weld joining two or more machine or tool elements is often undertaken. These are plane or axisymmetric elements working in conditions of loading. The shape optimization of plane or axisymmetric elements is directed to minimize their stress concentration factor. This problem is undertaken in the works of Dig (1986), Fiacco and McCormich (1968), Francavilla *et al.* (1975) and Na *et al.* (1983).

A lot of the published papers on optimization problems use the finite element method to analyse the structure (see the works of Dems and Mróz (1978), Dems (1980), and Dig (1986 for instance). In order to generate any boundary shape it is postulated that the constitutive parts are either circles or straight lines. The whole boundary is defined by the data of particular points, some of which are mobile (see Braibat and Fleury (1984), and Bhavikatti and Ramakrishnan (1980)). Shape optimization is more complex than pure sizing optimization. Since the shapes are continuously changing in the design process, a careful consideration has to be paid to describe the changing boundary shape. In this paper the following problem is analysed. It considers two machine cylindrical elements which are first welded and then subjected to machining. The problem is to determine the shape of the weld surface between two cylindrical elements of different diameters and thermal stresses arising from the welding process.

The shape optimization problem can be stated as

$$\min_{\mathbf{V}} \{\phi(\mathbf{V}) = \max \sigma_{\text{von Mises}}\} \tag{1}$$

subject to the following inequality constraints:

$$\begin{aligned} &m_i(\mathbf{V}) \leqslant 0; \quad i = 1, \ldots, NBC \\ &V_k^{\mathrm{L}} \leqslant V_k \leqslant V_k^{\mathrm{U}}; \quad k = 1, \ldots, NSV \\ &d_j \leqslant \sum_{k=1}^{NSV} d_{kj} V_k \leqslant d_i, \quad j = 1, \ldots, NGC \end{aligned} \tag{2}$$

where ϕ is the objective function, m_i the constraint function describing the ith structural response, $\mathbf{V}$ a vector defining the shape of the structure, V_k^{L} and V_k^{U} are the lower and the upper limits of the shape variables which may reflect fabrication or analysis limitations, d_j and d_{kj} are shape variables, NBC the number of behavioural constraints, NSV the number of shape variables, and NGC the number of geometrical constraints. V_k will be considered as the global coordinate vector describing the structural shape. Then d_j and d_{kj} are shape variables, which depend on the moving directions of the control nodes.

THERMAL STRESS ANALYSIS

At this point the theory for welding stress calculations is briefly presented. Those readers interested in other theoretical aspects similar to those presented here can acquaint themselves with details given in the works of Argyris *et al.* (1977, 1978, 1981, 1982, 1985) and Kleiber and Służalec (1983, 1984). Consider the equilibrium equation. The quasi-static motion of an elementary volume is governed by the rate form of equilibrium between stress $\dot{\boldsymbol{\sigma}}$ and body forces $\dot{\mathbf{p}}$

$$\operatorname{div} \dot{\boldsymbol{\sigma}} + \dot{\mathbf{p}} = 0. \tag{3}$$

For thermoelastic–viscoplastic material behaviour the stress rate is derived from the additive decomposition of the total strain rate $\dot{\boldsymbol{\gamma}}$ into elastic $\dot{\boldsymbol{\varepsilon}}$, viscoplastic $\dot{\boldsymbol{\eta}}_{\mathrm{vp}}$, and thermal $\dot{\boldsymbol{\eta}}_{\mathrm{T}}$ strain rate components

$$\dot{\boldsymbol{\gamma}} = \dot{\boldsymbol{\varepsilon}} + \dot{\boldsymbol{\eta}}_{\mathrm{vp}} + \dot{\boldsymbol{\eta}}_{\mathrm{T}} \tag{4}$$

where

$$\dot{\boldsymbol{\varepsilon}} = \underline{\mathcal{E}}^{-1}\dot{\boldsymbol{\sigma}} \tag{5}$$

$$\dot{\boldsymbol{\eta}}_{\mathrm{vp}} = \frac{\mu}{3}\left(\frac{\bar{\sigma}^2}{\sigma_{\mathrm{y}}} - 1\right)\boldsymbol{\sigma}_{\mathrm{d}} \tag{6}$$

$$\dot{\boldsymbol{\eta}}_{\mathrm{T}} = \boldsymbol{\alpha}\Delta T \tag{7}$$

$$\bar{\sigma}^2 = \tfrac{3}{2}\boldsymbol{\sigma}_{\mathrm{d}}^{\mathrm{T}}\boldsymbol{\sigma}_{\mathrm{d}} \tag{8}$$

μ is the viscosity, σ_{y} the yield stress, $\boldsymbol{\sigma}_{\mathrm{d}}$ the stress deviator, $\boldsymbol{\alpha}$ the thermal expansion coefficient, ΔT the temperature increment, and superscript T denotes the transpose vector.

The viscoplastic yield surface is assumed

$$f(\boldsymbol{\sigma}, \boldsymbol{\eta}_{\mathrm{vp}}, T) = \tfrac{3}{2}\boldsymbol{\sigma}_{\mathrm{d}}^{\mathrm{T}}\boldsymbol{\sigma}_{\mathrm{d}} - \sigma_{\mathrm{y}}^2 > 0 \tag{9}$$

and the hardening rule

$$\sigma_{\mathrm{y}}(\boldsymbol{\eta}_{\mathrm{vp}}, T) = \frac{C(T)\bar{\eta}_{\mathrm{vp}}}{(1 + (C(T)\bar{\eta}_{\mathrm{vp}}\sigma_{\mathrm{m}}(T))^{m})^{m}} \tag{10}$$

where

$$\bar{\eta}_{\mathrm{vp}}^2 = \tfrac{2}{3}\boldsymbol{\eta}_{\mathrm{vp}}^{\mathrm{T}}\boldsymbol{\eta}_{\mathrm{vp}}.$$

The values of the functions $C(T)$ and $\sigma_{\mathrm{m}}(T)$ can be obtained from the uniaxial test (see Argyris *et al.*, 1977, 1978, 1981, 1982, 1985 for instance). The spatial discretization of the quasi-static motion with finite element expansions of the displacement field leads to the well-known equations of incremental equilibrium for the unknown nodal velocities $\dot{\mathbf{U}}$

$$\underline{K}\dot{\mathbf{U}} = \dot{\mathbf{P}}_1 + \dot{\mathbf{P}}_2 \tag{11}$$

where $\underline{K}$ denotes the stiffness matrix as a function of the current temperature field, $\mathbf{P}_1$ represents the thermal driving force due to thermal straining, and $\mathbf{P}_2$ the residual forces due to the elastic stress.

SHAPE OPTIMIZATION

Geometric and mechanical relationships

Recall that the fundamental finite element equation for the solid element describing the relationships between displacements and loads is of the form based on the textbook of Zienkiewicz (1977)

$$\underline{K}\mathbf{U} = \mathbf{P} \tag{12}$$

where $\underline{K}$ is the structural stiffness matrix, $\mathbf{U}$ the unknown nodal displacement vector, and $\mathbf{P}$ the generalized load vector. Both $\underline{K}$ and $\mathbf{P}$ are function of the shape variables V_k. Equations (12) and (13) are two linear systems of equations. A specific displacement $\mathbf{s}$ can be expressed as a linear combination of $\mathbf{U}$

$$\mathbf{s} = \underline{q}\mathbf{U} \tag{13}$$

where $\underline{q}$ is a constant matrix for all load cases.

The stress vector at a certain point in one of the structural finite elements can also be expressed as

$$\boldsymbol{\sigma} = \underline{q}^{\sigma}\mathbf{U} \tag{14}$$

where $\underline{q}^{\sigma}$ is the element stress matrix depending on the element nodal forces and on the element stiffness matrix.

Differentiating eqn (12) with respect to V_k

$$\frac{\partial \mathbf{U}}{\partial V_k} = \underline{K}^{-1}\left(\frac{\partial \mathbf{P}}{\partial V_k} - \frac{\partial \underline{K}}{\partial V_k}\mathbf{U}\right) = \underline{K}^{-1}\mathbf{F}_{\mathrm{p}} \tag{15}$$

where

$$\mathbf{F}_{\mathrm{p}} = \frac{\partial \mathbf{P}}{\partial V_k} - \frac{\partial \underline{K}}{\partial V_k}\mathbf{U} \tag{16}$$

represents a pseudo-load matrix.

Differentiating eqns (13) and (14) with respect to V_k furnishes

$$\frac{\partial \mathbf{s}}{\partial V_k} = \underline{q}\underline{K}^{-1}\mathbf{F}_{\mathrm{p}} \tag{17}$$

$$\frac{\partial \boldsymbol{\sigma}}{\partial V_k} = \frac{\partial \underline{q}^{\sigma}}{\partial V_k}\mathbf{U} + \underline{q}^{\sigma}(\underline{K}^{-1}\mathbf{F}_{\mathrm{p}}). \tag{18}$$

Equations (17) and (18) can also be written in another form

$$\frac{\partial \mathbf{s}}{\partial V_k} = \mathbf{F}_{\mathrm{p}}\mathbf{V}^{*} \tag{19}$$

$$\frac{\partial \boldsymbol{\sigma}}{\partial V_k} = \frac{\partial \underline{q}^{\sigma}}{\partial V_k}\mathbf{U} + (\mathbf{F}_{\mathrm{p}}\underline{V}_{*}^{\sigma}) \tag{20}$$

where

$$\begin{aligned} \underline{V}^{*} &= \underline{K}^{-1}\underline{q} \\ \underline{V}_{*}^{\sigma} &= \underline{K}^{-1}\underline{q}^{\sigma} \end{aligned} \tag{21}$$

represent the virtual displacement matrices under virtual loads $\underline{K}^{-1}\underline{q}$ and $\underline{K}^{-1}\underline{q}^{\sigma}$, respectively.

Analysing the geometric relationships one can recall that assuming global displacements $\mathbf{u}$ for any point in a two-dimensional finite element, one has

$$\mathbf{u} = \underline{N}\mathbf{U} \tag{22}$$

where $\mathbf{U}$ is the vector of nodal displacements and $\underline{N}$ the shape function matrix. The form of $\underline{N}$ can be found in the textbook of Zienkiewicz (1977) for instance. The strain for any point is

$$\varepsilon = \underline{B}\mathbf{U} \tag{23}$$

where the form of the matrix $\underline{B}$ is given by Zienkiewicz (1977) for instance. The element stiffness is taken from the work of Zienkiewicz (1977)

$$\underline{K} = \int_{\Omega} \underline{B}^{\mathrm{T}} \underline{Q} \underline{B} \, \mathrm{d}\Omega = \sum_{k} \underline{B}^{k\mathrm{T}} \underline{Q} \underline{B}^{k} \det \underline{J}^{k} W_{k} \tag{24}$$

where $\underline{Q}$ is the corresponding elastic or elastic–plastic matrix, Ω the volume of the finite element, k stands for the Gaussian integration points, $\det \underline{J}^{k}$ the Jacobian determinant, and W^{k} the weighting coefficient at k.

The nodal force vector is

$$\mathbf{P} = \int_{\partial\Omega} \underline{N}^{\mathrm{T}} \mathbf{f} \, \mathrm{d}(\partial\Omega) = \sum_{k} \underline{N}^{k\mathrm{T}} \mathbf{f}^{k} \det \underline{J}^{k} W^{k} \tag{25}$$

where $\mathbf{f}$ is the vector of forces acting on surface $\partial\Omega$. Supposing that mechanical properties of the material are prescribed and do not change during the optimization process, then the derivatives of the objective function, and $\underline{K}$, $\underline{q}^{\sigma}$ and $\mathbf{P}$ for each element with respect to the shape variable V_{k} can be obtained in the following way:

$$\frac{\partial \underline{q}^{\sigma}}{\partial V_{j}} = \underline{Q} \frac{\partial \underline{B}}{\partial V_{j}} \tag{26}$$

where

$$\frac{\partial \underline{B}}{\partial V_{j}} = \sum_{i=1}^{NEN} \left(\frac{\partial \underline{B}}{\partial X_{i}} \cdot \frac{\partial X_{i}}{\partial V_{j}} + \frac{\partial \underline{B}}{\partial Y_{i}} \cdot \frac{\partial Y_{i}}{\partial V_{j}} \right) = \sum_{i} \left(\left(\frac{\partial \underline{B}}{\partial X_{i}} \frac{\partial \underline{B}}{\partial Y_{i}} \right) \frac{\partial}{\partial V_{j}} \begin{bmatrix} X_{i} \\ Y_{i} \end{bmatrix} \right) \tag{27}$$

X_{i}, Y_{i} show the element nodes, and NEN is the number of element nodes.

Based on $\partial \underline{B}/\partial V_{j}$ one obtains

$$\begin{aligned} \frac{\partial \underline{K}}{\partial V_{j}} &= \frac{\partial}{\partial V_{j}} \left(\sum_{k} \underline{B}^{k\mathrm{T}} \underline{Q} \underline{B}^{k} \det J^{k} W^{k} \right) \\ &= \sum_{k} \left(\frac{\partial B^{k\mathrm{T}}}{\partial V_{j}} \underline{Q} \underline{B}^{k} \det \underline{J}^{k} W^{k} + \underline{B}^{k\mathrm{T}} \underline{Q} \frac{\partial \underline{B}^{k}}{\partial V_{j}} \det J^{k} W^{k} \right. \\ &\quad \left. + \underline{B}^{k\mathrm{T}} \underline{Q} \underline{B}^{k} \frac{\partial \det \underline{J}^{k}}{\partial V_{j}} W^{k} \right), \quad j = 1, \ldots, NMN \end{aligned} \tag{28}$$

where NMN is the number of master nodes

$$\frac{\partial \mathbf{P}}{\partial V_j} = \sum_k \underline{N}^{k\mathrm{T}} \frac{\partial}{\partial V_j} (\mathbf{f}^k \det \underline{J}^k) W^k, \quad j = 1, \ldots, NMN. \tag{29}$$

Shape representation

The method used to describe the shape of the structure is the key element in the process of obtaining the optimum shape. In this paper boundary nodes are used for shape representation. Use of coordinates for boundary nodes in the finite element model as shape variables is the earliest method used. The approach is simple and instinctive, and associated with the finite element method (Prasad and Haftka, 1979).

Solution method

The shape optimization problem represented by eqn (1) can be transformed into a sequential unconstrained optimization problem by using an extended penalty function like in the works of Dig (1986), Queau and Trompette (1980), and Ramakrishnan and Francavilla (1974). It may be written as

$$\min_{\mathbf{V}} \Lambda(\mathbf{V}, r) = \phi(\mathbf{V}) + rG(\mathbf{V}) \tag{30}$$

where

$$G(\mathbf{V}) = \sum_j (g_j(\mathbf{V}))^{-1} \quad \text{if} \quad g_j(\mathbf{V}) \geqslant g_0$$

$$G(\mathbf{V}) = \sum_j (2 - g_j(\mathbf{V}) g_0^{-1}) g_0^{-1} \quad \text{if} \quad g_j(\mathbf{V}) < g_0$$

g_0 is a constant called the transition parameter, r the response factor, and $g_j(\mathbf{V})$ the constraint functions. For further details refer to the papers of Dig (1986) and Queau and Trompette (1980).

NUMERICAL EXAMPLE

In practice, welding stresses and deformations in all points of the welded joint should be in the elastic range. External loading should lead to additional elastic stresses. Therefore, such a model of the welded joint is analysed in this paper. It should be noted that sometimes plastic deformations within the weld can appear. Consider two thick-walled cylindrical elements which have to be joined by a welding process. A scheme and the dimensions of these elements are presented in Fig. 1. The properties of the base material and the filler metal assumed for numerical analysis are given in Figs 2 and 3. The elements after the

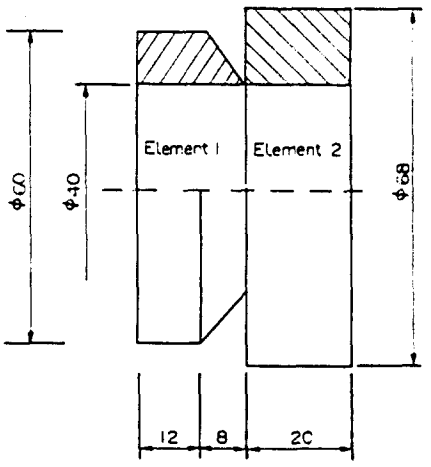

Fig. 1. Dimensions of two cylindrical elements subjected to welding.

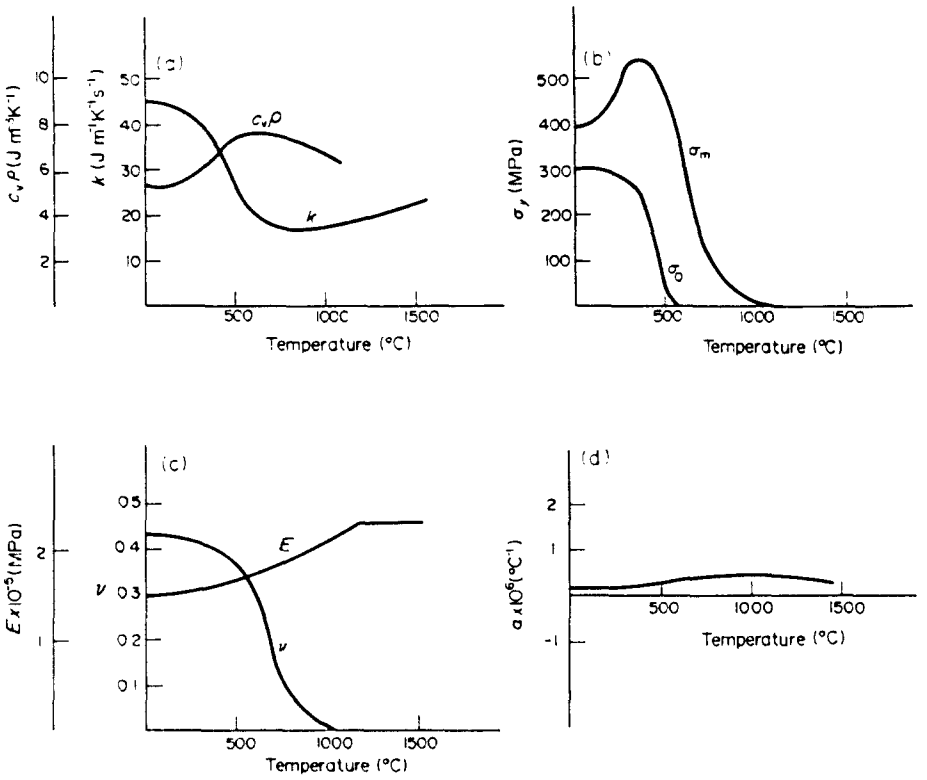

Fig. 2. Properties of the base material assumed for the analysis: (a) thermal conductivity $k(T)$ and heat capacity $c_v\rho(T)$; (b) initial $\sigma_0(T)$ and maximum yield limit $\sigma_m(T)$; (c) elastic modulus $E(T)$ and Poisson's ratio $\nu(T)$; (d) linear coefficient of thermal expansion $\alpha(T)$.

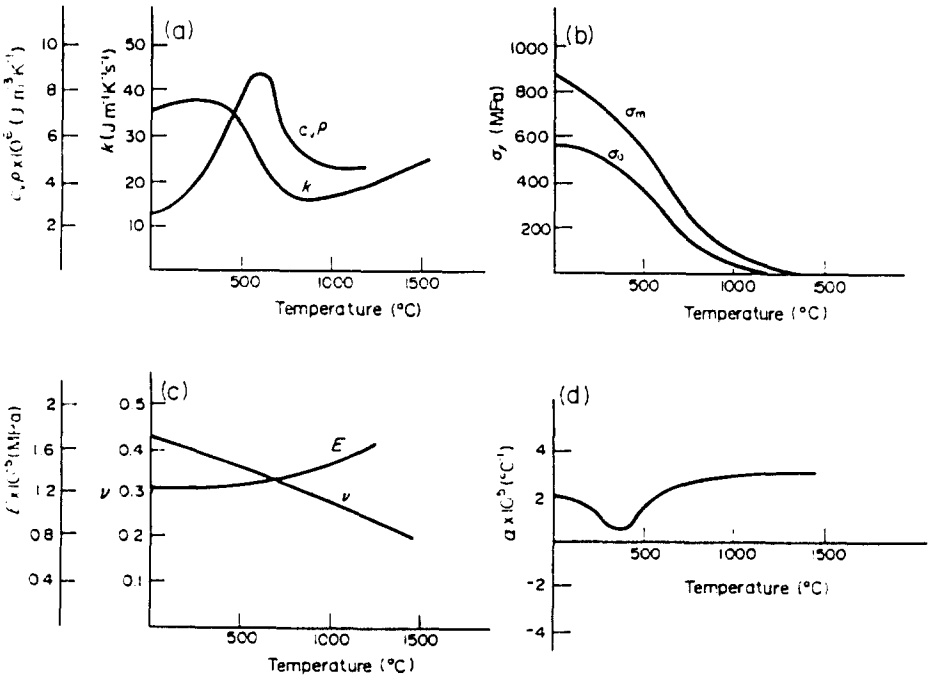

Fig. 3. Properties of the filler metal assumed for the analysis: (a) thermal conductivity $k(T)$ and heat capacity $c_v\rho(T)$; (b) initial $\sigma_0(T)$ and maximum $\sigma_m(T)$ yield limit; (c) elastic modulus $E(T)$ and Poisson's ratio $\nu(T)$; (d) linear coefficient of thermal expansion $\alpha(T)$.

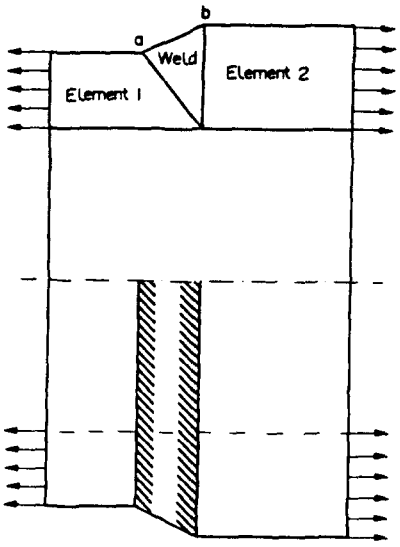

Fig. 4. Cylindrical elements after welding before machining undergoing axial loading.

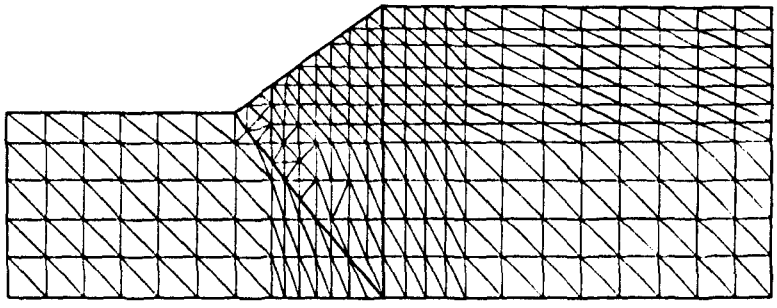

Fig. 5. Finite element axisymmetric mesh used.

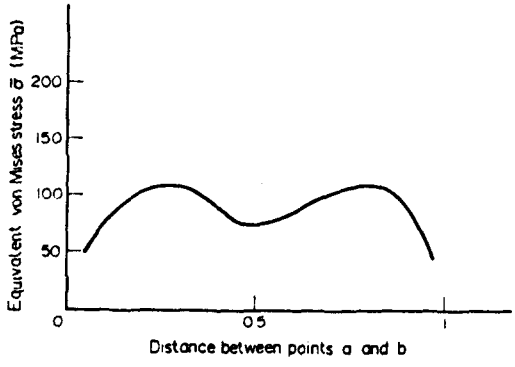

Fig. 6. Residual stress distribution on line a–b after welding.

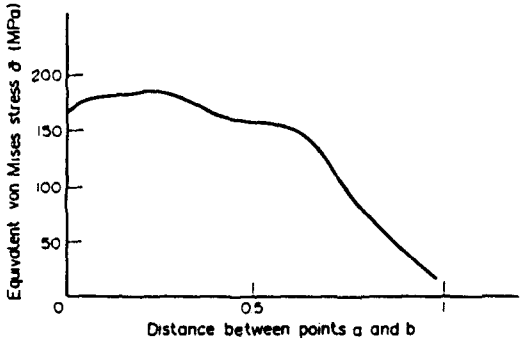

Fig. 7. Stresses on line a–b with external loading.

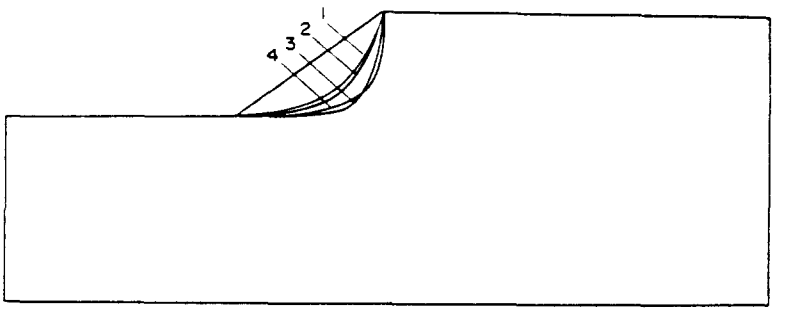

Fig. 8. An analysis of optimal shape of the weld. Curves 1–4 show the steps in the optimization process.

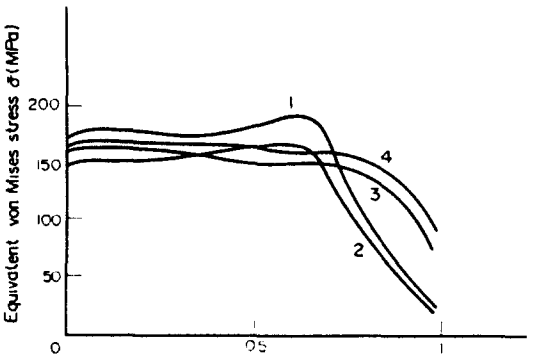

Fig. 9. The distribution of stresses for steps 1–4 shown in Fig. 8.

welding process are shown in Fig. 4. For the analysis of welding stresses the finite element mesh shown in Fig. 5 is used. This mesh was also used for an optimal design of the shape. Simple triangular elements with linear shape functions are used here. The following conditions of welding were discussed: gross heat input, 1.6 MJ m $^{-1}$; assumed number of passes, 1. Figure 6 supplies information concerning residual stresses after welding. Figure 7 presents stresses on the analysed boundary line in the weld, i.e. between points a and b in Fig. 4 for an external loading of 60 MPa. As can be seen the stress distribution in the weld is not proper.

This is the reason that by using a machining process one should change the weld line and try to decrease stress concentration on this boundary line. It should be noted that additional stresses obtained by the machining process are not analysed here. Figure 8 shows different shapes for determining a machining process and indicates the optimal shape of the weld. Curves 1–4 show the steps in the optimization process. Figure 9 presents the distribution of stresses on line a–b (see Fig. 4) for different shapes of these lines. It can be seen that the most advantageous shape is that presented in Fig. 8—curve 4. Equivalent von Mises stress for this curve varies over a small range. For the considered joint this kind of weld shape should be used in welding constructions.

CONCLUDING REMARKS

The optimization problems have practical significance and application in welding processes. The work of welding construction depends mainly on the proper design of the weld. This paper shows how one can use computer methods to improve the stress distribution in welds joining axisymmetric machine elements. The paper indicates the method of the analysis for various kinds of welds and gives an example for the butt joint. Deformations in the weld are normally in the elastic range. Therefore one can use the linear model for optimizing the shape of the weld.

REFERENCES

Argyris, J. H., Szimmat, J. and William, K. J. (1982). Computational aspects of welding stress analysis. *Comput. Meth. Appl. Mech. Engng* **33**, 635–666.

Argyris, J. H., Szimmat, J. and Willam, K. J. (1985). Finite element analysis of arc-welding process. In *Numerical Methods in Heat Transfer* (Edited by R. W. Lewis), Vol. III. Wiley, New York.

Argyris, J. H., Vaz, L. E. and Willam, K. J. (1977). Higher order methods for transient diffusion analysis. *Comput. Meth. Appl. Mech. Engng* **12**, 243–278.

Argyris, J. H., Vaz, L. E. and Willam, K. J. (1978). Improved solution methods for inelastic rate problems. *Comput. Meth. Appl. Meth. Engng* **16**, 231–277.

Argyris, J. H., Vaz, L. E. and Willam, K. J. (1981). Integrated finite element analysis for coupled thermo-viscoplastic problems. *J. Thermal Stresses* **4**, 121–153.

Bhavikatti, S. S. and Ramakrishnan, C. V. (1980). Optimum shape design of rotating disc. *Comput. Struct.* **11**, 397–401.

Braibat, V. and Fleury, C. (1984). Shape optimal design using *B*-spline. *Comput. Meth. Appl. Mech. Engng* **44**, 247–267.

Dems, K. (1980). Multiparameter shape optimization of elastic bars in torsion. *Int. J. Numer. Meth. Engng* **15**, 1517–1539.

Dems, K. and Mróz, Z. (1978). Multiparameter structural shape optimization by the finite element method. *Int. J. Numer. Meth. Engng* **13**, 247–263.

Dig, Y. (1986). Shape optimization of structures: a literature survey. *Comput. Struct.* **24**, 985–1004.

Fiacco, A. V. and McCormich, G. E. (1968). *Nonlinear Programing Sequential Unconstrained Minimization Techniques*. Wiley, New York.

Francavilla, A., Ramakrishman, C. V. and Zienkiewicz, O. C. (1975). Optimization of shape to minimize stress concentration. *J. Strain Analysis* **10**, 63–70.

Kleiber, M. and Służalec, A. (1983). Numerical analysis of heat flow in flash welding. *Arch. Mech.* **35**, 687–699.

Klewiber, M. and Służalec, A. (1984). Finite element analysis of heat flow in friction welding. *Engng Trans.* **32**, 107–113.

Na, M. S., Kikichi, N. and Taylor, J. E. (1983). Optimal modification of shape for two-dimensional elastic bodies. *J. Struct. Mech.* **11**, 11–135.

Prasad, B. and Haftka, R. T. (1979). Optimal structural design with plate finite elements. *J. Struct. Div., ASCE* ST11, 2367–2382.

Queau, J. P. and Trompette, P. (1980). Two-dimensional shape optimal design by the finite element method. *Int. J. Numer. Meth. Engng* **15**, 1603–1612.

Ramakrishnan, C. V. and Francavilla, A. (1974). Structural shape optimization using penalty functions. *J. Struct. Mech.* **3**, 403–422.

Zienkiewicz, O. C. (1977). *The Finite Element Method*. McGraw-Hill, New York.

Zienkiewicz, O. C. and Campbell, J. S. (1973). Shape optimization and sequential linear programming. In *Optimum Structural Design* (Edited by R. H. Gallagher and O. C. Zienkiewicz). Wiley, New York.